Journal of the Mechanical Behavior of Biomedical Materials xxx (xxxx) xxx–xxx

Contents lists available at ScienceDirect

Journal of the Mechanical Behavior of Biomedical Materials

journal homepage: www.elsevier.com/locate/jmbbm

Kinematics of collagen fibers in carotid arteries under tension-inflation loading

Witold Krasny[a,b,c,d], Hélène Magoariec[d], Claire Morin[a,b,c], Stéphane Avril[a,b,c,*]

[a] Ecole Nationale Supérieure des Mines de Saint-Etienne, CIS-EMSE, SAINBIOSE, F-42023 Saint Etienne, France
[b] INSERM, U1059, F-42000 Saint Etienne, France
[c] Université de Lyon, SAINBIOSE, F-42000 Saint Etienne, France
[d] Laboratoire de Tribologie et Dynamique des Systèmes, CNRS UMR 5513, Université de Lyon, Ecole Centrale Lyon, France

ARTICLE INFO

Keywords:
Carotid artery
Tension-inflation
Collagen
Adventitia
Fiber bundles
Reorientation
Kinematics

ABSTRACT

Biomechanics of the extracellular matrix in arteries determines their macroscopic mechanical behavior. In particular, the distribution of collagen fibers and bundles plays a significant role. Experimental data showed that, in most arterial walls, there are preferred fiber directions. However, the realignment of collagen fibers during tissue deformation is still controversial: whilst authors claim that fibers should undergo affine deformations, others showed the contrary. In order to have an insight about this important question of affine deformations at the microscopic scale, we measured the realignment of collagen fibers in the adventitia layer of carotid arteries using multiphoton microscopy combined with an unprecedented Fourier based method. We compared the realignment for two types of macroscopic loading applied on arterial segments: axial tension under constant pressure (scenario 1) and inflation under constant axial length (scenario 2). Results showed that, although the tissue underwent macroscopic stretches beyond 1.5 in the circumferential direction, fiber directions remained unchanged during scenario 2 loading. Conversely, fibers strongly realigned along the axis direction for scenario 1 loading. In both cases, the motion of collagen fibers did not satisfy affine deformations, with a significant difference between both cases: affine predictions strongly under-estimated fiber reorientations in uniaxial tension and over-estimated fiber reorientations during inflation at constant length. Finally, we explained this specific kinematics of collagen fibers by the complex tension-compression interactions between very stiff collagen fibers and compliant surrounding proteins. A tensegrity representation of the extracellular matrix in the adventitia taking into account these interactions was proposed to model the motion of collagen fibers during tissue deformation.

1. Introduction

The arterial tissue exhibits a hierarchical microstructure, made of three concentric layers, namely, starting from the arterial lumen towards the external surface of the vessel: the intima, the media, and the adventitia. The extracellular matrix of these three layers is made of arrangements of collagen and elastin fiber networks, with a specific organization depending on the layer. In particular, the non-linear mechanical behavior of the arterial tissue is often associated with the progressive rearrangements of these different fiber networks, at the 10–100 μm scale. In the present contribution, we chose to focus on the adventitial collagen, since it was recently shown to be the fiber network the most prone to mechanically-induced rearrangements (Schrauwen et al., 2012; Chen et al., 2013; Sugita and Matsumoto, 2017; Krasny et al., 2017). In particular, this network, composed of thick bundles of type I collagen fibers (Dingemans et al., 2000), is the major structural component of the adventitia, due to its important load-bearing function preventing over-distensions (Humphrey, 2002). Eventually, its remodeling under pathological situations such as aneurysms may degrade this load bearing function (Humphrey and Canham, 2000).

Various experimental loading setups coupled to live microscopy provided a better understanding of the fiber kinematics, allowing progressive improvements of structural constitutive models of the arterial wall. Namely, in the unloaded configuration, the adventitial collagen network shows randomly distributed orientations and a high degree of crimping (Dingemans et al., 2000; O'Connell et al., 2008; Rezakhaniha et al., 2012). Upon mechanical loading, the collagen bundles progressively unfold (Canham et al., 1992; Greenwald et al., 1997). The measurement of fiber waviness (Chen et al., 2011; Schrauwen et al., 2012; Wang et al., 2013; Sugita and Matsumoto, 2017) revealed in

* Corresponding author at: Ecole Nationale Supérieure des Mines de Saint-Etienne, CIS-EMSE, SAINBIOSE, F-42023 Saint Etienne, France.
E-mail address: avril@emse.fr (S. Avril).

http://dx.doi.org/10.1016/j.jmbbm.2017.08.014
Received 17 May 2017; Received in revised form 7 August 2017; Accepted 9 August 2017

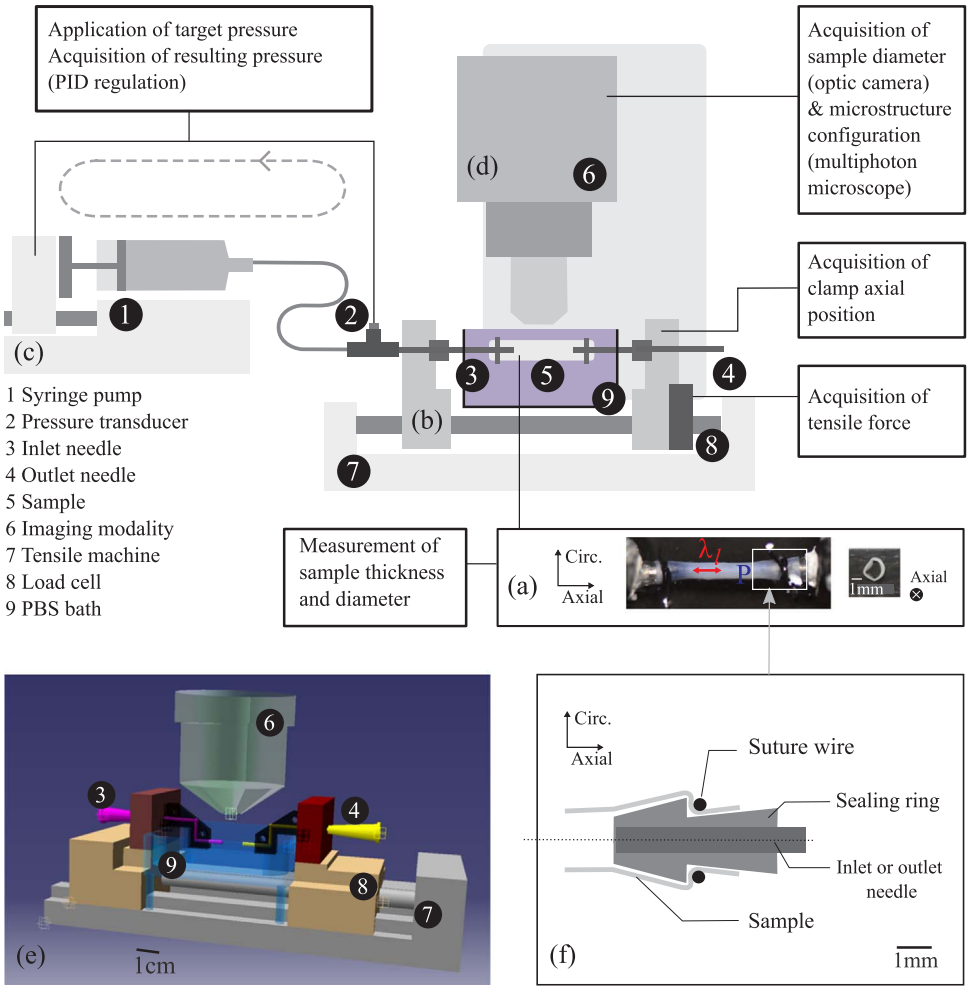

Fig. 1. Experimental tension-inflation setup showing (a) a sample cannulated on the needles and loaded, comprising of (b) the tensile machine, (c) the syringe pump, (d) imaging modalities (alternatively optical camera and multiphoton microscope); (e) a schematic representation of the tension-inflation setup, showing the tensile machine, the PBS bath in blue transparency, needle stiffening casings in black transparency, inlet (pink) and outlet (green) needles, the multiphoton microscopes objective in grey (center); and (f) a section sketch of the cannulated arterial sample for tension-inflation testing, presenting the sealing method. (For interpretation of the references to color in this figure legend, the reader is referred to the web version of this article.)

particular that recruitment, or engagement of collagen fibers, is gradual (unsynchronized among fibers) and starts at a finite strain (Hill et al., 2012; Chow et al., 2014). The process can differ whether the observed vascular region is close or remote from the heart (distal regions vs. proximal regions) (Zeinali-Davarani et al., 2015). Collagen fiber bundles may also undergo a progressive realignment in response to the application of a macroscopic deformation (Arkill et al., 2010; Keyes et al., 2011; Chen et al., 2011; Chow et al., 2014; Krasny et al., 2017). This realignment has been observed to take place after recruitment, in order for the artery to continue deforming without damaging the engaged fibers (Wang et al., 2013), and showed discrepancies in fiber realignment amplitudes, depending on the initial fiber angle and on the type of deformation (Wan et al., 2012; Chen et al., 2013). The fiber bundles are finally stretched upon further mechanical loading. Eventually, rupture of the collagen fibers may lead to the rupture of the adventitial layer. Consequently, a correct assessment of the mechanical fields within the adventitia relies on a correct description of the collagen network and of its evolution during loading.

The aforementioned experimental findings enhanced the first generation of structural models based on the definition of a strain energy function, which considered the arterial wall as a soft matrix material reinforced by variously distributed fibers families (Holzapfel and Gasser, 2001; Zulliger et al., 2004; Holzapfel et al., 2005; Gasser and Holzapfel, 2007), with the addition of a fiber activation stretch or of a probability distribution function, accounting for gradual recruitment at finite strain (Roy et al., 2011; Hill et al., 2012). All these models assume an affine deformation of the collagen network, as experimentally evidenced by several contributions (Sacks, 2003; Wan et al., 2012), i.e. the fibers are assigned to follow the overall material deformation: they are firmly embedded in the surrounding matrix. The resulting understanding of collagen kinematics and its integration in structural models provides today satisfactory predictions of the artery's mechanical response (Zulliger et al., 2004; Holzapfel et al., 2005). However, questions remain about the microscopic mechanisms governing the observed rearrangements. The latter question is especially raised with regards to past studies, revealing non-affine collagen kinematics (Billiar and Sacks, 1997; Chandran and Barocas, 2006; Jayyosi et al., 2016; Krasny et al., 2017), illustrating the complexity of arterial microstructure properties. Whether they are attributed to the decrimping process (Lee et al., 2015), to fiber-fiber interactions (Chow et al., 2014) or to fiber-matrix interactions (Billiar and Sacks, 1997; Thorpe et al., 2013), non-affine collagen kinematics are currently taken into account in a novel generation of multiscale and micromechanical modelling approaches (Stylianopoulos and Barocas, 2007; Fan and Sacks, 2014; Zhang et al., 2013; Morin et al., 2015), but their microstructural and micromechanical origin has not yet been experimentally documented nor understood, which constitutes a limit for further refined multi-scale formulations. Specifically, few studies investigate the dependence of fiber kinematics on the loading type (Wan et al., 2012; Chen et al., 2013), and to the authors' knowledge, none have quantitatively compared fiber rotations for the same tracked fibers undergoing different loading scenarii, while comparing them to affine predicted reorientations. In the present study, we bridge this gap by answering the following questions: do particular deformation scenarii or conditions challenge affinity of fiber motion? Is the fibers' behavior different under the different loading scenarii? To this aim, we submitted carotid arteries from New Zealand White rabbits to tension-inflation tests, while quantitatively characterizing the reorientations of their adventitial

collagenous microstructure with multi-photon microscopy.

2. Materials and methods

2.1. Sample preparation

Carotid arteries (n = 4) were harvested at the Veterinary Campus of the Université de Lyon (VetAgro Sup, Marcy l'Étoile, FR) from healthy male New Zealand White rabbits, weighing 3 kg approximately. The cadavers, kindly provided by Centre Lago (Vonnas, FR), were previously sacrificed under compliance with the NIH Guide for Care and Use of Laboratory Animals. Immediately after excision, the samples were stored in a bath of phosphate-buffered saline (10x PBS, pH 7.1) at 5 °C and tested within 36 h after harvesting. For each sample, a 15 ± 1 mm long cylindrical segment was extracted for mechanical testing (Fig. 1(a), left image) as well as three 0.5 mm long rings for optical measurement of the sample thickness (Fig. 1(a), right image). The sample tips were cannulated onto the inlet and outlet needles using suture wire (Fig. 1(a)). Two plastic rings previously fixed on the needles at the suture loci (Fig. 1(f)) prevented slipping during axial tension and provided a waterproof sealing during inflation. The sealing rings provided structural support to sustain axial tension and no damage was observed on the samples at the locus of the ring after the mechanical tests.

2.2. Mechanical setup

We hereafter describe the mechanical setup that enabled tension-inflation of the carotid arteries. Applying an axial tension was made possible by a screw-driven high precision tensile machine (Deben® Microtest tensile/compression stage) equipped with a 150 N load cell (Fig. 1(b) and 1(e)) which provided a 0.01 N precision with satisfactory stability during the tests. The two heads of the machine moved in opposite directions, allowing the operator to identify and keep track of a region of interest, while the microscope was positioned at the center of the sample. The force offset was zeroed prior to the mounting of the sample. Verifying that the axial force and sample length were unchanged after mounting allowed limiting the risk of potential pre-strain and pre-stress in the sample. A pressure loading was applied by a syringe pump (Fig. 1(c)) (Harvard Apparatus®) equipped with a ± 300 mmHg pressure transducer (FISO® optical fiber connected to the fluid network at the sample inlet) which infused phosphate-buffered saline (10x PBS, pH 7.1) at a constant ambient temperature of 20 °C. Applying a target pressure was made possible by the pump and pressure transducer communicating under closed loop control (PID mode). The settings of the proportional gain and integrator constants were iteratively adjusted in order to obtain a stable pressure step, characterized by a reasonable pressurizing time and limited overshooting. During the mechanical loading, the sample was continuously immerged in PBS at a constant ambient temperature of 20 °C (Fig. 1(b)). Also, the pressure readouts at inlet and outlet were compared to ensure that the pressure was uniformly distributed and did not vary due to friction forces in the needles during infusion. An optical camera (Nikon® D7200 equipped with Nikon® AF-S VR Micro-Nikkor optical 105 mm f/2.8G IF-ED lens) was used to acquire images of the deforming arterial sample and of the three sample rings, for subsequent analysis of sample diameter and sample thickness (Fig. 1(a)). Noticeably, the measurement of the arteries' diameter showed a limited variability along the sample length (standard deviations being as low as 2% of the measured mean diameters).

2.3. Multiphoton microscopy

The multiphoton microscope (NIKON, A1R MP PLUS®) of the IVTV platform (Engineering and Ageing of Living Tissues Platform, ANR-10-EQPX-06-01, Lyon, FR) was used to image the fibrous microstructure of the tested arterial segments (Fig. 1(d)), without prior staining or fixation. Using a 870 nm excitation wavelength (Hill et al., 2012), the collagen second harmonic generation (SHG) signal was acquired through 400–492 nm band-pass filters. The multiphoton imaging modality was well documented in previous studies (Van Zandvoort et al., 2004; O'Connell et al., 2008; Sugita and Matsumoto, 2017), should additional information be needed. The imaging resolution of the microscope was set to 0.5 µm in all directions (Hill et al., 2012; Schrauwen et al., 2012) with a 512 µm² imaging window. An optimal compromise was achieved between image quality and acquisition time by setting the scan speed to 0.5 frames per second, with two-frame averaging. These setting resulted in 60–90 µm thick stacks of images with acquisition times of approximately 15 min. A period of 5 min was always observed after applying an incremental load step to the artery in order to stabilize the tissue before imaging it. However, this apparent creeping occurring after each load step applied on the arterial tissue did not change the microstructural morphology of the tissue, as observed by live imaging.

2.4. Loading scenario and data acquisition

In agreement with well-established tension-inflation protocols for arteries (Humphrey, 2002; Keyes et al., 2011), two loading scenarii were considered, namely axial tension under constant imposed pressure and inflation under constant axial stretch. Four carotids were used in the present study, carotid samples S1 and S2 were tested under both loading scenarii, while carotid samples S3 and S4 were tested under only one loading scenario, i.e. the axial tension and the inflation scenario, respectively. For each sample and each loading scenario, the loading protocol was composed of three loading steps (Fig. 2). Step 1 consisted in five preconditioning cycles, carried out in order to cancel the tissue's deformation history, step 2 consisted in one loading cycle dedicated to the acquisition of macroscopic sample dimensions, and step 3 consisted in one final loading cycle dedicated to the acquisition of the collagen load-dependent morphologies, by means of multiphoton microscopy. As a result, on the one hand, three samples (S1, S2, and S3) underwent a total of seven axial tension cycles (with the two last cycles dedicated to data acquisition) between 0.1 ± 0.02 and 0.8 ± 0.02 N axial force, at an imposed velocity of 2 mm·min^{-1}, corresponding to an axial strain rate of 0.2 min^{-1}, with maintained pressure (P = 100 mmHg). On the other hand, three samples (S1, S2, and S4) underwent a total of seven inflation cycles (with the two last cycles dedicated to data acquisition) between 20 and 140 mmHg, by steps of 20 mmHg imposed within 30 s, under a maintained *in vivo* axial stretch (λ_a = 1.6 ± 0.05). The *in vivo* stretch, defined as the stretch resulting in unchanged axial reaction force during inflation (Humphrey, 2002), was determined by adjusting the clamp position during the preconditioning cycles. The samples reference cross-sectional areas A_0 were computed from the measures of the unloaded sample diameters after preconditioning (Step 1 of the protocol) and from the initial thicknesses. In the case of the axial tension load scenario, the zero axial strain position was obtained from the axial position at which the axial force returned to zero after preconditioning. The measurement of the sample length after preconditioning provided the reference length l_0 on the basis of which the macroscopic axial stretch was computed as $\lambda_a = l/l_0$. l and l_0 refer to the current and the reference inter-clamp lengths of the sample, respectively. Similarly, in the case of the inflation loading scenario, the zero circumferential strain position was obtained from the measurement of the sample diameter after preconditioning, when the inflation system was opened, forcing the pressure to return to 0 mmHg in the sample. The measurement provided the reference diameter D_0 on the basis of which the macroscopic circumferential stretch was computed as $\lambda_c = D/D_0$. D and D_0 refer to the current and the reference diameters of the sample, respectively. After preconditioning, the gauge length of the samples (between suture) measured l_0 = 12 ± 2 mm, while the unloaded sample diameter measured D_0 = 2.0 ± 0.3 mm. Macroscopic

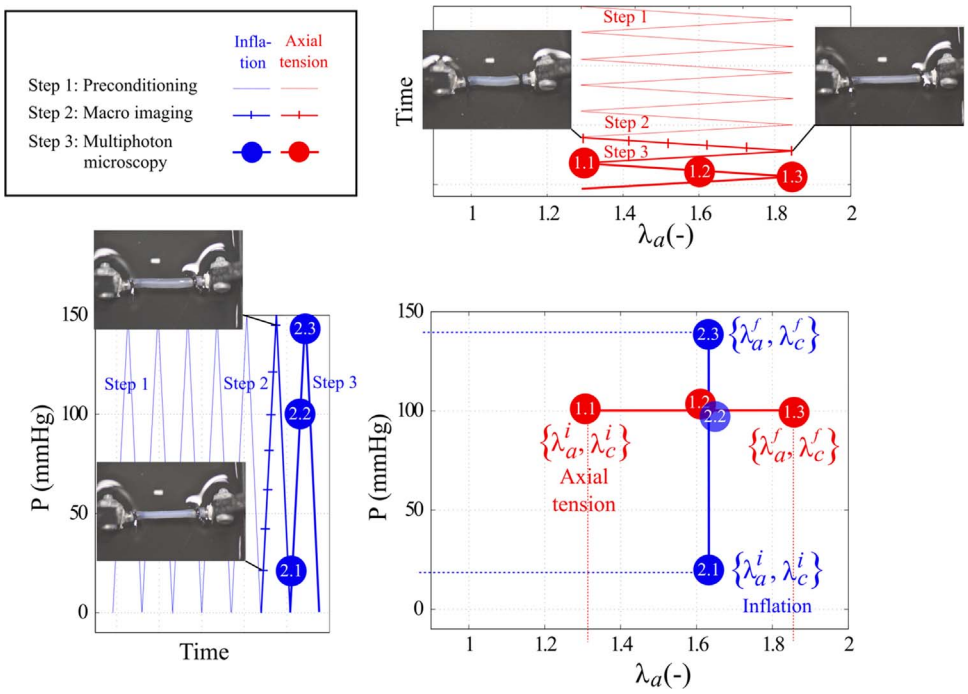

Fig. 2. Tension-inflation loading protocol, comprised of three loading steps for both axial tension and inflation scenario, namely Step 1: preconditioning (thin line), Step 2: macroscopic imaging sequence (thick line with ticks denoting macro images), and Step 3: multiphoton microscopy sequence (thick line with circles denoting loading configurations in which the collagen morphology was acquired). The morphologies referring to load states 1.1, 1.3, 2.1 and 2.3 are used as inputs for subsequent image processing and fiber kinematics characterization (see Section 2.5 and Fig. 3). The five preconditioning cycles, the macroscopic diameter acquisition cycle, and the microscopy acquisition cycle are represented as function of time. The tensile loading scenario is represented in red, whereas the inflation loading scenario is represented in blue. (For interpretation of the references to color in this figure legend, the reader is referred to the web version of this article.)

images of the samples (Step 2 of the loading protocol) were obtained every 20 mmHg during inflation and every 0.5 mm during axial tension, corresponding to 0.2 ± 0.05 stretching steps approximately (see thick lines with ticks on Fig. 2, showing macroscopic imaging). Microscopy images (Step 3 of the protocol) were obtained at 1.3 ± 0.05, 1.6 ± 0.05, and 1.8 ± 0.05 stretches during axial tension (referenced as loading configurations 1.1, 1.2, and 1.3, respectively (Fig. 2)), and at 20 mmHg, 100 mmHg, and 140 mmHg pressures during inflation (referenced as loading configurations 2.1, 2.2, and 2.3, respectively (Fig. 2)). The mechanical configurations 1.1 and 2.1 will be referred to in the following as “reference configurations”, while the mechanical configurations 1.3 and 2.3 will be referred to as “loaded configurations”. As concerns the intermediate loading configurations 1.2 and 2.2, they were not used in the Fourier methodology enabling the characterization of fiber kinematics affinity but provided a refined insight into the evolution of the microstructure during the loading (see Fig. 4 in Section 3), and a verification of the right tracking of the same imaging windows. The reference configurations included partial loading (λ_a = 1.3, P = 100 mmHg for scenario 1, λ_a = 1.6, P = 20 mmHg for scenario 2) for several reasons. First, we chose to post-process adventitial collagen images characterized by a sufficient degree of decrimping, hence avoiding imprecisions in the Fourier analysis of the global orientations of the fibers (at the bundle scale); second, this choice prevented the potential buckling of the samples at high pressure and low axial stretch (Han et al., 2013), which could have impaired the analysis of macroscopic and microscopic kinematics.

2.5. Image analysis and characterization of fiber kinematics

The previously collected mechanical and microstructural information was used to analyze the fiber rearrangements and the corresponding fiber kinematics for the different loading scenarii.

Firstly, image stacks corresponding to the reference configurations 1.1 and 2.1 (Fig. 2), as well as image stacks corresponding to the loaded configurations 1.3 and 2.3 (Fig. 2), were processed using a Maximum Intensity Projection (MIP) algorithm (Fig. 3 (a1) and (a2)), revealing optimal in-plan morphology. In fact, previous studies have investigated the transmural angle (radial direction) of the fibers in the arterial adventitia and showed that it is negligible in comparison to the in-plane angle (Roy et al., 2011; Rezakhaniha et al., 2012; Schrauwen et al., 2012). As a result, although the negligible transmurality information is lost, the fibers are represented with maximal effective length, strongly improving the interpretation of their in-plane orientation. A preliminary geometrical analysis revealed that the potential evaluation error of in-plane fiber orientation caused by projecting slices of a cylinder into a 2D image, was always under 5% (maximal at the image periphery, where the tangential plane shows the highest inclination to the projection plane), and hence was considered negligible.

Secondly, the affine transformation was simulated, by numerically applying axial and circumferential deformations to the reference configurations. In more details, for the loading scenario 1 (axial tension under constant pressure), a numerical axial stretch λ_a^* together with the corresponding measured transverse contraction (resulting from diameter change) λ_c^* were gradually applied to the image of the reference configuration 1.1 (Fig. 2). Similarly, for loading scenario 2 (inflation under constant axial stretch), a numerical circumferential stretch λ_c^* (corresponding to outer diameter change) was gradually applied to the image of the reference configuration 2.1 (Fig. 2). Image resolution remained unchanged by the use of subpixel interpolation.

Afterwards, the 2D Fourier spectrum moduli were extracted from the collagen morphologies for both the numerically deformed (Fig. 3 (c1)) and the experimentally loaded configurations (Fig. 3 (c2)). Use of the 2D Fourier transforms allowed removing the non-mechanical optical effects (such as contrast or brightness effects) as well as the artifacts (features occurring at short lengthscale, such as the decrimpring process), and the inequality of imaged windows. Previous studies have proven the potential of the Fast Fourier transform (FFT 2D) for the analysis of biomedical images, and in particular the ability of the method to extract fiber angle densities or isotropy parameters (Ayres et al., 2006; D'Amore et al., 2010; Schriefl et al., 2012; Polzer et al., 2013; Chow et al., 2014; Morrill et al., 2016). Here a special attention was paid to work with spectra being matrices of identical dimensions (Fig. 3, red cropping square). A preliminary analysis allowed verifying that the locus of the cropping center in the image did not affect the results. Each spectrum was then multiplied by the Fourier transform of a Gaussian window whose size corresponded to the characteristic width of a collagen bundle (1/25 of the imaged window, equivalent to 20 μm), allowing the filtering of undesirable small-length features in

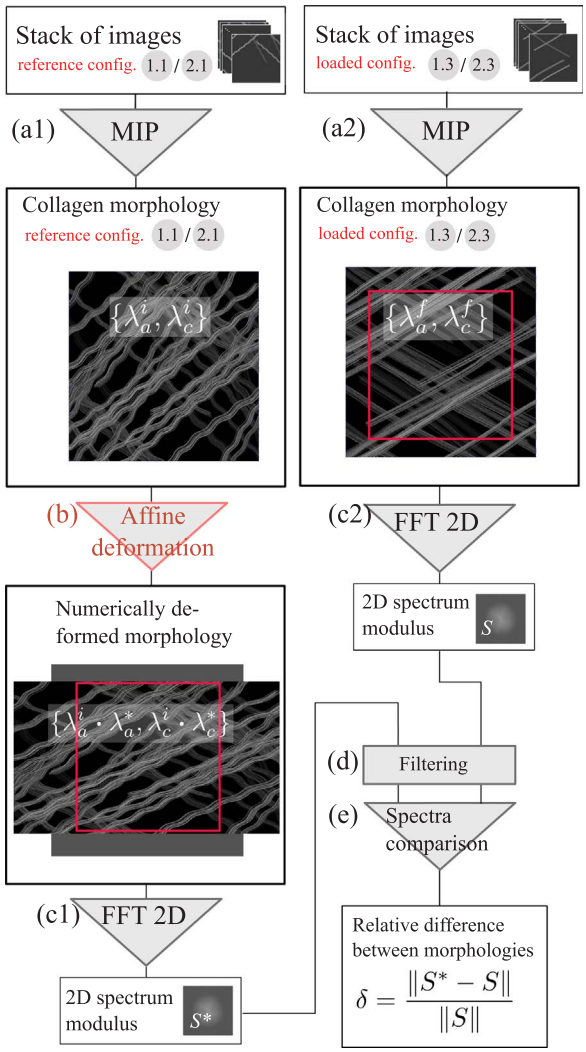

Fig. 3. Series of operations summarizing the image analysis and characterization methodology of fiber kinematics. The methodology consisted in (i) analyzing the stacks of images in the reference (a1) and loaded (a2) configurations by means of a Maximum Intensity Projection (MIP); (ii) numerically applying a gradual affine deformation to the reference configurations (b); and (iii) comparing the microstructure configurations through their FFT spectra (c), so as to extract the affine deformation (applied numerically), which produced a microstructure with minimum relative difference between the experimental morphology and the numerically deformed one (d). For each loading scenario, the axial stretch ranged between λ_a^i (reference configuration) and λ_d^f (loaded configuration) ($\lambda_a^i = \lambda_d^f$ in the case of the inflation loading), whereas the circumferential stretch ranged between λ_c^i (reference configuration) and λ_c^f (loaded configuration). In this figure, the used images are custom-drawn visual representations of collagen morphology, chosen for clarity and representativeness.

the images and the highlighting of meaningful morphological features (namely fiber orientations at the scale of the bundles) (Fig. 3 (d)) (Zisserman, 2014). The obtained 2D Fourier spectrum moduli S* and S (numerically and experimentally deformed microstructures, respectively) were finally compared using a relative norm-2 (Fig. 3 (d)).

We gradually increased the numerically applied affine deformation, eventually reaching a minimum in the relative difference between the two collagen morphologies (i.e. configurations 1.3 or 2.3 and the corresponding affine deformations of configurations 1.1 and 2.1, Fig. 2). As a result, this minimum corresponded to the application of a fictitious stretch that should be applied to the reference microstructure in order to reach by affine deformation the most similar microstructure to the loaded experimental configuration. Eventually, this fictitious stretch was compared to the actual experimentally measured stretch. If the fictitious stretch and the actual stretch are equal, then the kinematics at the scale of collagen fibers actually remained affine.

3. Results

First, we qualitatively compared the microstructure evolution between the two loading scenarii (Fig. 4). Fig. 4(a) shows that, under axial tension at a constant intermediate pressure, adventitial collagen fibers achieved full straightening and reoriented towards the macroscopic strain direction. On the contrary, Fig. 4(b) shows that, under inflation at the *in vivo* stretch, collagen fibers of the adventitia achieved full straightening but the orientation of the majority of the fibers remained unchanged. Similar images, and hence similar analyzes were obtained for the 2 other samples in each loading direction. Imaging always the same region of interest in the tissue at the different stages of the deformation made the characterization of fiber reorientations reliable.

As a second step, we quantitatively analyzed the kinematics of the fiber rotation for each loading scenario (Fig. 5). For loading scenario 1 (corresponding to axial tension under constant imposed pressure), the difference δ between the numerical and the experimental morphologies started, for the three samples, at high values: this denotes different microstructure morphologies between the reference arterial configuration and axially loaded arterial configuration, particularly in terms of fiber orientations (Fig. 5(a1)). As the numerically applied affine deformation increased, the fibers gradually reoriented towards the direction of axial tension, hence coming closer to the experimental fiber orientations of the loaded configuration: the relative difference δ between the spectra decreased. When the applied affine deformation became too high, the relative difference increased again: affine deformation induced fiber rotations being larger than the ones experimentally observed (Fig. 5(a3)). In between, the relative difference δ reached a minimum value, when the fibers of the experimentally and the numerically deformed configurations showed the closest fiber orientations (Fig. 5(a2)). For the three tested samples S1, S2, and S3, δ reached its minimum at axial stretch values comprised between 1.86 and 2.05, i.e. to obtain similar morphologies, the numerically applied stretch needs to be, in average, 14% higher than the experimentally applied stretch (Fig. 5, black dots). For loading scenario 2, δ starts, for the three samples, at very low values: this denotes similar microstructure morphologies between the reference and the loaded arterial configurations, particularly in terms of fiber orientations (Fig. 5(b1)). As the numerically applied circumferential stretch increased, the fibers reoriented towards the circumferential load direction, hence driving away from the fiber orientations of the experimentally loaded configuration: this led to a continuously increasing relative difference δ between the spectra (Fig. 5(b2) and (b3)). For the three tested samples S1, S2, and S4, the minimum of δ was reached at circumferential stretch values comprised between 1.10 and 1.12, i.e. to have comparable morphologies, the numerically applied stretch needs to be, in average, 25% lower than the experimentally applied stretch.

4. Discussion

The mechanically-induced reorientation of collagen fibers was the focus of several contributions, studying different collageneous tissues, such as tendon (Lake et al., 2012), collagenous constructs (Chandran and Barocas, 2006), skin (Bancelin et al., 2015; Lynch et al., 2017), bovine pericardium (Billiar and Sacks, 1997), liver capsule (Jayyosi et al., 2016), and carotid artery (Krasny et al., 2017). The debated question concerns the affine character of the reorientation process: do the fibers follow the strain imposed by their surrounding matrix, or are other mechanisms active in the reorientation process? The previously cited studies showed that collagen fibers present complex and potentially non-affine kinematics under load. However, while the reorientation of collagen fibers has been widely characterized, none of the contributions had investigated the effect of loading types on fiber kinematics while characterizing the affine character of the fiber

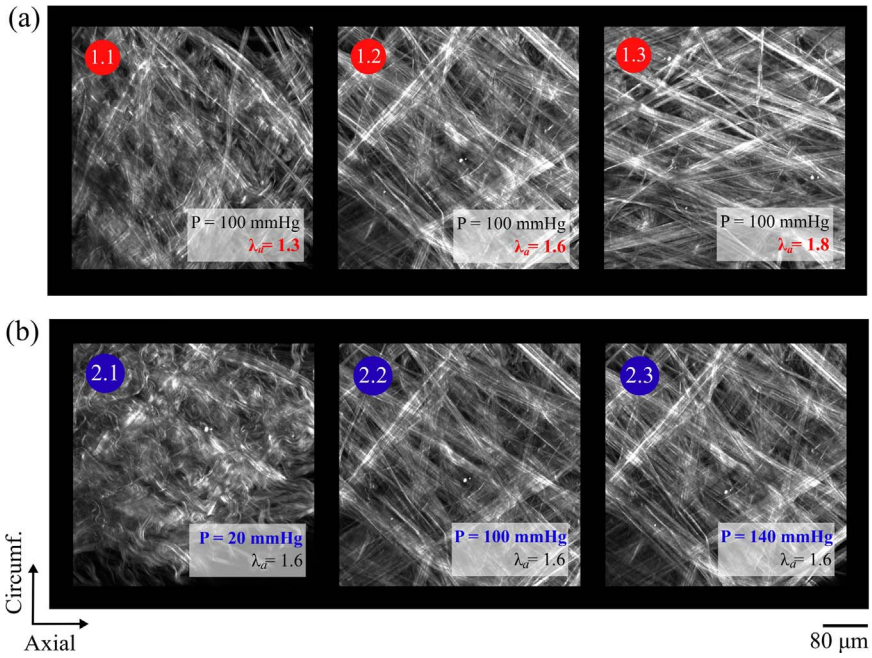

Fig. 4. Adventitial collagen morphology under both loading scenarii, revealed through multiphoton microscopy for sample S1: (a) tension under imposed constant pressure and (b) inflation under imposed constant axial stretch.

reorientations. However, the results collected in the present paper suggest that the loading scenario, and more precisely the local strain tensor, plays an important role on bundle kinematics. We therefore propose to compare our results to the other available studies, paying a special attention to the loading scenario which was imposed to the arterial tissue.

In the present contribution, we investigated the kinematics of adventitial collagen bundles, when subjecting the arterial tissue to two different loading scenarii, namely axial tension under constant pressure and inflation under constant axial stretch, while the microscopic configuration of adventitial collagen was acquired by means of multiphoton microscopy. Regarding the first loading scenario, maintaining a constant pressure (P = 100 mmHg) while applying axial stretches produced a pronounced reorientation of adventitial collagen fibers. To our best knowledge, the contribution the closest to ours is the one of Chen et al. (2013), who studied the behavior of collagen fibers of coronary arteries under axial tensile loading while maintaining a constant circumferential stretch. In these tests, fiber reorientations showed limited reorientations (their rotation being 13% lower than predicted by the affine kinematics). The discrepancy with our results may originate in that, under such a deformation, no transverse strain of the sample is possible (through the use of a balloon catheter). In the present study however, the transverse strain observed while applying an axial tension to the samples S1, S2, and S3 was measured as 15%, 18%, and 18%, respectively. As a result, the deformations applied by Chen et al. (2013) induced a different strain state within the tissue as compared to our protocol. This may explain the different fiber kinematics.

We also investigated the fiber kinematics under inflation tests at a constant imposed axial strain. The applied methodology for the characterization of fiber kinematics suggests that inflating the artery at the constant *in vivo* length does not produce noticeable rotations of collagen fibers in the adventitia. Collagen fibers first straighten (engagement) and then keep their orientation unchanged. A similar result was obtained by Schrauwen et al. (2012), who submitted carotid arteries to inflation after applying an initial stretch of $\lambda_a = 1.5$. They measured fiber waviness and orientation across a given region of interest. Results showed that after unfolding (waviness parameter >0.8, corresponding to an applied pressure of 60 mmHg), the peak orientation density did not vary further during the deformation (maximum pressure 120 mmHg), indicating that fibers did not reorient during deformation. Microscopy images also suggested, that the global orientations of the crimped fibers did not vary noticeably during the decrimping process occurring early in the inflation procedure (0–60 mmHg). Also, in the contribution of Chen et al. (2013) and despite the different type of artery, adventitial collagen was shown to behave similarly to our results. Referring to the presented results (Chen et al., 2013) and interpreting fiber reorientations under increasing circumferential stretches ($\lambda_c = 1$ to $\lambda_c = 1.7$) at a given axial stretch ($\lambda_a = 1.5$), which is a loading scenario kinematically equivalent to inflation at constant axial stretch, we note that fibers showed limited reorientations (their rotation being 30% lower than predicted by the affine kinematics). To our best knowledge, only Keyes et al. (2011) obtained results with different trends although applying an analogous mechanical protocol. They found that adventitial collagen fibers reorient significantly from axial to circumferential directions under high pressure. These differences may be attributed to a different tissue type and a different methodology, given that a fixed region of interest was not tracked during the overall microscopy procedure of these authors.

The kinematics of collagen bundles is also modified when the applied loading scenario induces yet other macroscopic strains. Indeed, Wan et al. (2012) compared three inflation configurations (increasing internal pressure) while simultaneously reducing axial stretch. They found that collagen in mouse adventitia shows affine kinematics in the physiological range of deformations. Furthermore, Sacks (2003) documented collagen kinematics under planar biaxial deformation with conclusions supporting the affine assumption for fiber kinematics, i.e. fibers following the macroscopic strain. In a previous study (Krasny et al., 2017), we focused on uniaxial tensile tests of strips of carotid arteries, showing that collagen bundles reorient faster than predicted by affine kinematics. The discrepancies between the presented results and those of the latter studies most certainly lie in different mechanical protocols, inducing different strain paths.

The complex rearrangements of collagen fibers under macroscopic loading raise the question of the underlying mechanisms governing their complex kinematics. While fiber uncrimping is intrinsically a non-affine mechanism (Fan and Sacks, 2014; Lee et al., 2015), we show in the present study that the non-affine character of collagen motion concerns also rigid motions of collagen fibers at the fiber lengthscale, regardless of its crimped or straight state. In order to explain the motion of collagen fibers, fiber-matrix interactions have to be taken into

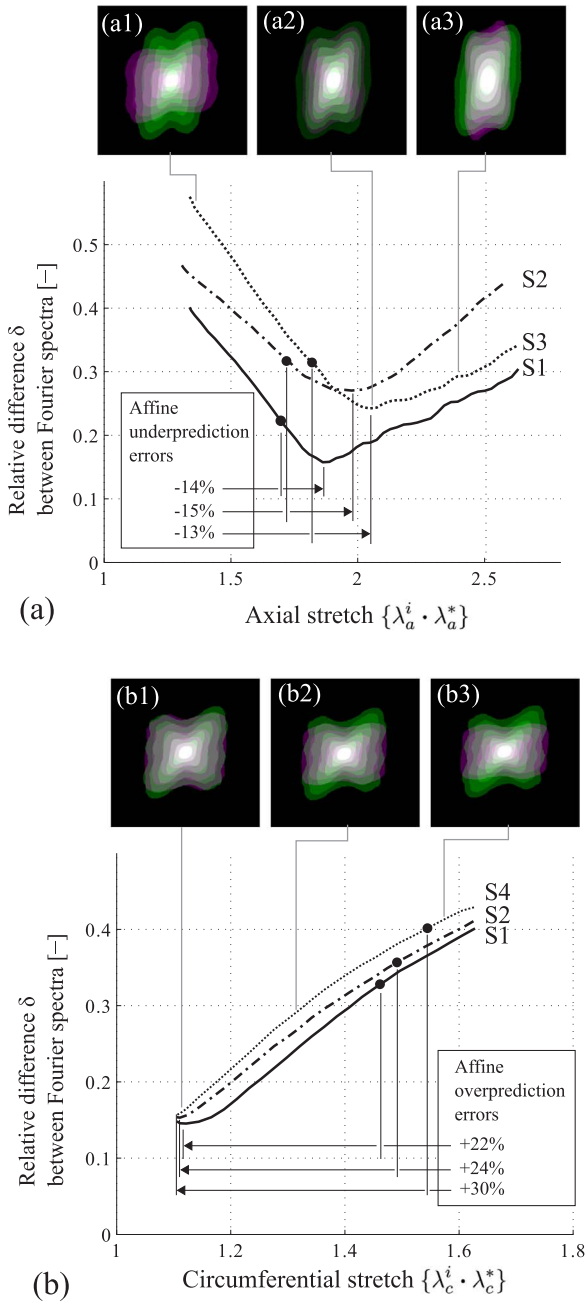

Fig. 5. Evolution of the relative difference δ between spectra corresponding to the numerically deformed morphology and the experimentally deformed morphology. (a) Loading scenario 1 (axial tension under constant imposed pressure): evolution of δ with the stretch numerically applied in the longitudinal direction λ_a^*; (b) Loading scenario 2 (inflation under constant axial stretch): evolution of δ with the stretch numerically applied in the circumferential direction λ_c^*. On each plot, the three curves refer to the three tested samples (either S1, S2, and S3 or S1, S2, and S4) and black dots • indicate the experimentally applied stretches λ_a^f and λ_c^f. For each loading scenario, examples of superimposed spectra are provided for one carotid samples in (a1)–(a3) and (b1)–(b3) for different stretches numerically applied to the reference configuration. The purple (resp. green) spectrum corresponds to the numerically applied affine deformation (resp. to the experimentally applied loading). The difference between the experimental and the numerical stretches minimizing the difference between morphology spectra is represented by horizontal arrows in each figure. Accordingly, prediction errors of affine kinematics are quantified under both loading scenarii. Prediction errors are negative when affine kinematics underpredicts the experimental stretch, and positive when affine kinematics overpredicts the experimental stretch. (For interpretation of the references to color in this figure legend, the reader is referred to the web version of this article.)

account. Previous studies have investigated the role of the non-collagenous matrix in the micromechanics of soft biological tissues, hence influencing collagen kinematics (Billiar and Sacks, 1997; Thorpe et al., 2013). In particular, recent modelling results have suggested that the non-linear mechanical response of the tissue is due to structural effects (spin effects) of the fibers network in interaction with the surrounding matrix (Morin et al., 2015). Presumably, a redistribution of microscopic stress through proteoglycans distributed in the matrix (Thorpe et al., 2013) influences fiber motion, with potential inner sliding inside each collagen fiber being responsible for the tissue's plastic response (Lynch et al., 2017). Besides, fiber-fiber interactions have been considered both in experimental investigations (Chow et al., 2014) as in modelling formulations (Lanir, 1979; Stylianopoulos and Barocas, 2007; Cardamone et al., 2009; Morin et al., 2015). While Lanir (1979) proposed a schematic representation of the collagen and elastin network structure in generalized collagenous tissues, with collagen undulation induced by the elastin exerting compression on them, Chow et al. (2014) illustrated structural and mechanobiological interactions between fibers, eventually showing that, in porcine thoracic aortas, the elastic fibers are under tension and induce an intrinsic compressive stress on the collagen. From the modelling point of view, Stylianopoulos and Barocas (2007) showed that a network composed of straight fibers interacting with each other via freely rotating crosslinks, incorporated as structural description of a Representative Volume Element in a multiscale model, provides good predictions of arterial biomechanics. Concerning the contribution of Morin et al. (2015), the developed micromechanical model predicts the load-induced decrimping and rotations of the fibers and the subsequent stiffening of the mechanical behavior of a Representative Volume Element, accounting for both fiber-fiber interactions and fiber-matrix interactions, while introducing linear elastic constitutive behavior for fibers and matrix phases.

These observations, coupled to (i) the evidenced coexistence of collagen and elastin in the adventitial layer of arteries such as the rabbit carotid (Krasny et al., 2017) or the pig coronary artery (Chen et al., 2013), to (ii) findings about the load-bearing properties of collagen fibers (the elastic modulus of collagen fibers being greater than the elastic modulus of elastic fibers by a factor 10^3 (Wenger et al., 2007; Burton, 1954; Faury, 2001)) and to (iii) the current understanding of both collagen-elastin fiber interactions and rearrangements (Lanir, 1979; Chow et al., 2014; Ferruzzi et al., 2011; Wang et al., 2013), suggest possible links with the cellular tensegrity theory (Ingber et al., 1993; Stamenović et al., 1996; Stamenovic and Coughlin, 2000). The cellular tensegrity theory, developed for subcellular descriptions, proposes a representation of the cellular cytostructure through a network of high-strength microtubules, maintained in compression by a network of low-strength actin fibers under tension, the whole system being in static equilibrium in the absence of an external load. Such theory can be extended to collagenous networks as shown in Fig. 6, where a simplified tensegrity model inspired from Luo et al. (2008) and De Jager and Skelton (2004) is introduced to represent arterial adventitia with rigid collagen fibers and compliant links between the collagen fibers (Chow et al., 2014). Such a model may explain the results observed in the present study: under inflation loading at a constant axial stretch, fiber rotation is impossible, as it would imply a transverse strain, the fibers being rigid. Conversely, under axial tensile loading at a fixed inner pressure, fiber rotation is the only way to allow the extension. Noticeably, this model may also explain the results of Chen et al. (2013); namely when applying an axial tension while maintaining the circumferential stretch constant (hence disabling transverse strain), fiber rotations were limited and overpredicted by affine predictions. All in all, this representation of the adventitial microstructure, based on a previously applied tensegrity model (Luo et al., 2008; De Jager and Skelton, 2004), could explain the complex kinematics of collagen fibers and their dependence on the type of loading scenario that we observed in the present study.

Still, several limitations to this study should be mentioned. In fact,

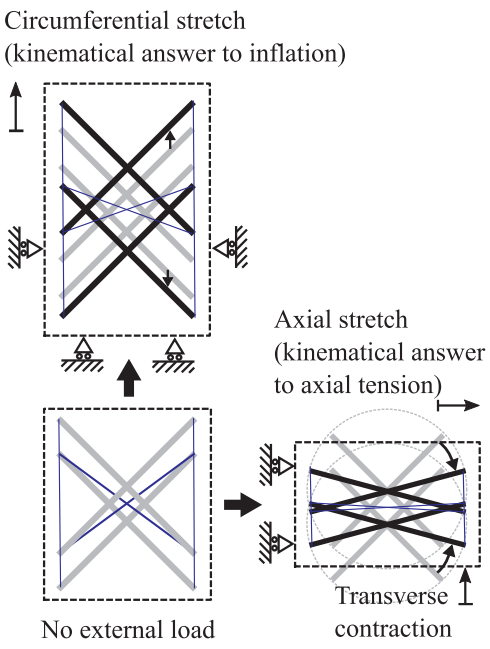

Fig. 6. Schematic representation of adventitial microstructure inspired from the tensegrity structure of Luo et al. (2008). Black segments represent here low-compliant collagen bundles, while blue segments represent high-compliant binding fibers which exert compressive forces on the collagen bundles under zero external load. The two considered loading scenarii are represented, characterized by free transverse strain boundary condition in the case of scenario 1 (axial tension), and by fixed axial length boundary condition in the case of scenario 2 (inflation). The grey segments represent the initial positions of collagen bundles, before deformation, to be compared with final positions in black, after deformation.

the deformations undergone by the arterial samples match only partially the *in vivo* mechanical loading. This is obviously the case of axial tension under constant pressure, but also to a certain extent of inflation at a fixed *in vivo* stretch. Also, the test temperature was maintained at 20 °C, while it is 38–40 °C *in vivo* , and the deformation was applied under quasi static conditions, which cannot render the dynamic nature of the pulsatile loading *in vivo* (of the order of 1 Hz). Moreover, the applied range of pressure did not match the *in vivo* amplitude between systole and diastole, which ranges between 105 ± 15 and 125 ± 15 mmHg (Govyrin, 1957) in the rabbit artery. Besides, excision of the arterial tissue from its native environment initiated, prior to testing, the destructive action of degradative enzymes affecting collagen content. In the meantime, as the tissue was stored in PBS, it was prone to a modification of residual stress, as a result of the evolving fixed-charge density accumulated by proteoglycans (Azeloglu et al., 2008), eventually causing a swelling of the tissue. As a result, it cannot be neglected that this residual stress, resulting from sample storing in PBS, influences both the mechanical response and collagen fiber kinematics. However, the objective of our contribution was to investigate a possible dependence of fiber kinematics to different loading scenarii, rather than to characterize the fiber kinematics under *in vivo* conditions. As a result, the choice of test temperature and of pressure range did not impair our observations and conclusions. Concerning loading dynamics, the quasi-static deformation protocol with tissue preconditioning allowed live imaging under multiphoton microscopy with repeatable results, which would not be possible if a dynamic pulsatile loading would have been applied as it is the case *in vivo*. Another limitation concerns the application of a Maximum Intensity Projection (MIP) algorithm (see Section 2.5) to the 3D images stack and the resulting 2D morphology that we analyzed. Indeed, fibers localized on the most outer circumferential layers of the artery appeared the brightest and uninterrupted in the resulting 2D morphology. As for deeper fibers, they appeared eventually overlapped by the outer fibers, with a decreased contrast on the image. As a result, although they are identical from the biological point of view, the different fibers did not contribute to the overall image spectrum with the same weight. This limitation highlights the importance of following the same region of interest during the microscopy procedure, given that the discrepancy of contributions relative to the different fibers with regards to the resulting 2D spectrum is identical in the different compared projected (MIP) morphologies. Finally, a limitation originates in the spectral comparison between, on the one hand, a morphology characterized by a slight crimping of fiber, and on the other hand, a morphology characterized by fully engaged, straight fibers. In fact, when choosing the reference morphology for spectrum analysis, a part of the computed spectrum difference δ originates in the undulated character of the fibers, and another part originates in the different fiber orientations at the fiber bundle scale. A preliminary analysis of spectrum sensitivity, using fictitious collagen images, showed that the undulation contribution to the computed spectrum difference was negligible with regards to the orientation contribution, provided that the small lengthscales corresponding to fiber crimping were excluded from our analysis by the selective filtering procedure. However, this is not anymore true when fiber crimping is important, hindering an analysis of global bundle orientation (as it is the case in the unloaded configurations in Krasny et al. (2017)). As concerns the interpretation of the adventitial microstructure using a tensegrity model, it must be mentioned that, at this stage of knowledge about the arterial microstructure, its physical validity is conditioned by the verification of several assumptions. In particular, collagen bundles are not capable of supporting the compressive forces exerted by elastin (which results in their crimped state under zero external load). However, this role in the overall force equilibrium may be played by proteoglycans: due to their ability to trap water molecules along with the sodium ions that equilibrate their electric charge (Azeloglu et al., 2008; Buschmann and Grodzinsky et al., 1995), the hydrated proteoglycans provide a mechanical resistance to compression. Another assumption concerns the nature of the bindings between collagen and elastin, which should be characterized experimentally in the future.

Nevertheless, the original outcomes of the present study significantly contribute to a better understanding of arterial kinematics at the microscopic scale. From the experimental side, future work should characterize the interactions between collagen and other binding proteins such as elastin. From the modelling side, tensegrity models could represent arterial microstructure and its associated mechanics, and future work should further test their applicability at the tissue level with collagen, elastin, and proteoglycans as principal components (Fig. 6).

Acknowledgements

This work was supported by the ARC 2 “Bien-être et vieillissement” research program of the Auvergne-Rhône-Alpes region (FR), with financial contributions from ERC consolidator grant “Biolochanics” (647067), Research group MMV – Mécanique des Matériaux du Vivant (LTDS, CNRS UMR 5513), and the Institut Carnot Ingénierie@Lyon (I@L). The authors thank Prof. Eric Viguier (VetAgro Sup, Université de Lyon, FR), Dr. Caroline Boulocher (VetAgro Sup, Université de Lyon, FR) and Mr. Fabrice Desplanches (Centre Lago, Vonnas, FR) for their help in provision and excision of arterial specimen. Authors also thank the IVTV (ANR-10-EQPX-06-01) team and especially Ing. Ophélie Pollet for her support during the imaging process, as well as Dr. Damien Constant (Ecole Centrale Lyon, FR) for his technical contribution in the preparation of the mechanical setup.

Appendix A. Supplementary data

Supplementary data associated with this article can be found in the online version at http://dx.doi.org/10.1016/j.jmbbm.2017.08.014.

References

Arkill, K.P., Moger, J., Winlove, C.P., 2010. The structure and mechanical properties of collecting lymphatic vessels: an investigation using multimodal nonlinear microscopy. J. Anat. 216 (5), 547–555.

Ayres, C., Bowlin, G.L., Henderson, S.C., Taylor, L., Shultz, J., Alexander, J., Telemeco, T.A., Simpson, D.G., 2006. Modulation of anisotropy in electrospun tissue-engineering scaffolds: analysis of fiber alignment by the fast Fourier transform. Biomaterials 27 (32), 5524–5534.

Azeloglu, E.U., Albro, M.B., Thimmappa, V.A., Ateshian, G.A., Costa, K.D., 2008. Heterogeneous transmural proteoglycan distribution provides a mechanism for regulating residual stresses in the aorta. Am. J. Physiol.-Heart Circ. Physiol. 294 (3), H1197–H1205.

Bancelin, S., Lynch, B., Bonod-Bidaud, C., Ducourthial, G., Psilodimitrakopoulos, S., Dokládal, P., Allain, J.M., Schanne-Klein, M.C., Ruggiero, F., 2015. Ex vivo multiscale quantitation of skin biomechanics in wild-type and genetically-modified mice using multiphoton microscopy. Sci. Rep. 5 (17), 635.

Billiar, K., Sacks, M., 1997. A method to quantify the fiber kinematics of planar tissues under biaxial stretch. J. Biomech. 30 (7), 753–756.

Burton, A.C., 1954. Relation of structure to function of the tissues of the wall of blood vessels. Physiol. Rev. 34 (4), 619–642.

Buschmann, M., Grodzinsky, A., et al., 1995. A molecular model of proteoglycan-associated electrostatic forces in cartilage mechanics. J. Biomech. Eng. 117 (2), 179–192.

Canham, P.B., Whittaker, P., Barwick, S.E., Schwab, M.E., 1992. Effect of pressure on circumferential order of adventitial collagen in human brain arteries. Can. J. Physiol. Pharmacol. 70 (2), 296–305.

Cardamone, L., Valentin, A., Eberth, J., Humphrey, J., 2009. Origin of axial prestretch and residual stress in arteries. Biomech. Model. Mechanobiol. 8 (6), 431–446.

Chandran, P.L., Barocas, V.H., 2006. Affine versus non-affine fibril kinematics in collagen networks: theoretical studies of network behavior. J. Biomech. Eng. 128 (2), 259–270.

Chen, H., Liu, Y., Slipchenko, M.N., Zhao, X., Cheng, J.X., Kassab, G.S., 2011. The layered structure of coronary adventitia under mechanical load. Biophys. J. 101 (11), 2555–2562.

Chen, H., Slipchenko, M.N., Liu, Y., Zhao, X., Cheng, J.X., Lanir, Y., Kassab, G.S., 2013. Biaxial deformation of collagen and elastin fibers in coronary adventitia. J. Appl. Physiol. 115 (11), 1683–1693.

Chow, M.J., Turcotte, R., Lin, C.P., Zhang, Y., 2014. Arterial extracellular matrix: a mechanobiological study of the contributions and interactions of elastin and collagen. Biophys. J. 106 (12), 2684–2692.

D'Amore, A., Stella, J.A., Wagner, W.R., Sacks, M.S., 2010. Characterization of the complete fiber network topology of planar fibrous tissues and scaffolds. Biomaterials 31 (20), 5345–5354.

De Jager, B., Skelton, R.E., 2004. Symbolic stiffness optimization of planar tensegrity structures. J. Intell. Mater. Syst. Struct. 15 (3), 181–193.

Dingemans, K.P., Teeling, P., Lagendijk, J.H., Becker, A.E., 2000. Extracellular matrix of the human aortic media: an ultrastructural histochemical and immunohistochemical study of the adult aortic media. Anat. Rec. 258 (1), 1–14.

Fan, R., Sacks, M.S., 2014. Simulation of planar soft tissues using a structural constitutive model: finite element implementation and validation. J. Biomech. 47 (9), 2043–2054.

Faury, G., 2001. Function-structure relationship of elastic arteries in evolution: from microfibrils to elastin and elastic fibres. Pathol. Biol. 49 (4), 310–325.

Ferruzzi, J., Vorp, D., Humphrey, J.D., 2011. On constitutive descriptors of the biaxial mechanical behaviour of human abdominal aorta and aneurysms. J. R. Soc. Interface 8 (56), 435–450.

Gasser, T.C., Holzapfel, G.A., 2007. Finite element modeling of balloon angioplasty by considering overstretch of remnant non-diseased tissues in lesions. Comput. Mech. 40 (1), 47–60.

Govyrin, V., 1957. Measurement of arterial pressures in intact rabbits. Bull. Exp. Biol. Med. 44 (1), 896–897.

Greenwald, S., Moore, J., Rachev, A., Kane, T., Meister, J.J., 1997. Experimental investigation of the distribution of residual strains in the artery wall. J. Biomech. Eng. 119 (4), 438–444.

Han, H.C., Chesnutt, J.K., Garcia, J.R., Liu, Q., Wen, Q., 2013. Artery buckling: new phenotypes, models, and applications. Ann. Biomed. Eng. 41 (7), 1399–1410.

Hill, M.R., Duan, X., Gibson, G.A., Watkins, S., Robertson, A.M., 2012. A theoretical and non-destructive experimental approach for direct inclusion of measured collagen orientation and recruitment into mechanical models of the artery wall. J. Biomech. 45 (5), 762–771.

Holzapfel, G.A., Gasser, T.C., 2001. A viscoelastic model for fiber-reinforced composites at finite strains: continuum basis, computational aspects and applications. Comput. Methods Appl. Mech. Eng. 190 (34), 4379–4403.

Holzapfel, G.A., Sommer, G., Gasser, C.T., Regitnig, P., 2005. Determination of layer-specific mechanical properties of human coronary arteries with nonatherosclerotic intimal thickening and related constitutive modeling. Am. J. Physiol.-Heart Circ. Physiol. 289 (5), H2048–H2058.

Humphrey, J., 2002. Cardiovascular Solid Mechanics: Cells, Tissues, and Organs. Springer, New York.

Humphrey, J., Canham, P., 2000. Structure, mechanical properties, and mechanics of intracranial saccular aneurysms. J. Elast. Phys. Sci. Solids 61 (1–3), 49–81.

Ingber, D.E., et al., 1993. Cellular tensegrity: defining new rules of biological design that govern the cytoskeleton. J. Cell Sci. 104 (613–613).

Jayyosi, C., Coret, M., Bruyere-Garnier, K., 2016. Characterizing liver capsule microstructure via in situ bulge test coupled with multiphoton imaging. J. Mech. Behav. Biomed. Mater. 54, 229–243.

Keyes, J.T., Borowicz, S.M., Rader, J.H., Utzinger, U., Azhar, M., Geest, J.P.V., 2011. Design and demonstration of a microbiaxial optomechanical device for multiscale characterization of soft biological tissues with two-photon microscopy. Microsc. Microanal. 17 (02), 167–175.

Krasny, W., Morin, C., Magoariec, H., Avril, S., 2017. A comprehensive study of layer-specific morphological changes in the microstructure of carotid arteries under uniaxial load. Acta Biomater. 57, 342–351 15 July.

Lake, S.P., Hadi, M.F., Lai, V.K., Barocas, V.H., 2012. Mechanics of a fiber network within a non-fibrillar matrix: model and comparison with collagen-agarose co-gels. Ann. Biomed. Eng. 40 (10), 2111–2121.

Lanir, Y., 1979. A structural theory for the homogeneous biaxial stress-strain relationships in flat collagenous tissues. J. Biomech. 12 (6), 423–436.

Lee, C.H., Zhang, W., Liao, J., Carruthers, C.A., Sacks, J.I., Sacks, M.S., 2015. On the presence of affine fibril and fiber kinematics in the mitral valve anterior leaflet. Biophys. J. 108 (8), 2074–2087.

Luo, Y., Xu, X., Lele, T., Kumar, S., Ingber, D.E., 2008. A multi-modular tensegrity model of an actin stress fiber. J. Biomech. 41 (11), 2379–2387.

Lynch, B., Bancelin, S., Bonod-Bidaud, C., Gueusquin, J.B., Ruggiero, F., Schanne-Klein, M.C., Allain, J.M., 2017. A novel microstructural interpretation for the biomechanics of mouse skin derived from multiscale characterization. Acta Biomater. 50, 302–311.

Morin, C., Avril, S., Hellmich, C., 2015. The fiber reorientation problem revisited in the context of Eshelbian micromechanics: theory and computations. Pamm 15 (1), 39–42.

Morrill, E.E., Tulepbergenov, A.N., Stender, C.J., Lamichhane, R., Brown, R.J., Lujan, T.J., 2016. A validated software application to measure fiber organization in soft tissue. Biomech. Model. Mechanobiol. 15 (6), 1467–1478.

O'Connell, M.K., Murthy, S., Phan, S., Xu, C., Buchanan, J., Spilker, R., Dalman, R.L., Zarins, C.K., Denk, W., Taylor, C.A., 2008. The three-dimensional micro- and nanostructure of the aortic medial lamellar unit measured using 3D confocal and electron microscopy imaging. Matrix Biol. 27 (3), 171–181.

Polzer, S., Gasser, T.C., Forsell, C., Druckmüllerova, H., Tichy, M., Staffa, R., Vlachovsky, R., Bursa, J., 2013. Automatic identification and validation of planar collagen organization in the aorta wall with application to abdominal aortic aneurysm. Microsc. Microanal. 19 (06), 1395–1404.

Rezakhaniha, R., Agianniotis, A., Schrauwen, J.T.C., Griffa, A., Sage, D., Bouten, C.V.C., Van De Vosse, F.N., Unser, M., Stergiopulos, N., 2012. Experimental investigation of collagen waviness and orientation in the arterial adventitia using confocal laser scanning microscopy. Biomech. Model. Mechanobiol. 11 (3–4), 461–473.

Roy, S., Boss, C., Rezakhaniha, R., Stergiopulos, N., 2011. Experimental characterization of the distribution of collagen fiber recruitment. J. Biorheol. 24 (2), 84–93.

Sacks, M.S., 2003. Incorporation of experimentally-derived fiber orientation into a structural constitutive model for planar collagenous tissues. J. Biomech. Eng. 125 (2), 280–287.

Schrauwen, J.T.C., Vilanova, A., Rezakhaniha, R., Stergiopulos, N., van de Vosse, F.N., Bovendeerd, P.H.M., 2012. A method for the quantification of the pressure dependent 3D collagen configuration in the arterial adventitia. J. Struct. Biol. 180 (2), 335–342.

Schriefl, J., Reinisch, J., Sankaran, S., Pierce, D.M., Holzapfel, G.A., 2012. Quantitative assessment of collagen fibre orientations from two-dimensional images of soft biological tissues. J. R. Soc. Interface 9, 3081–3093.

Stamenovic, D., Coughlin, M.F., 2000. A quantitative model of cellular elasticity based on tensegrity. J. Biomed. Eng. 122 (1), 39–43.

Stamenović, D., Fredberg, J.J., Wang, N., Butler, J.P., Ingber, D.E., 1996. A microstructural approach to cytoskeletal mechanics based on tensegrity. J. Theor. Biol. 181 (2), 125–136.

Stylianopoulos, T., Barocas, V.H., 2007. Multiscale, structure-based modeling for the elastic mechanical behavior of arterial walls. J. Biomech. Eng. 129 (4), 611–618.

Sugita, S., Matsumoto, T., 2017. Multiphoton microscopy observations of 3D elastin and collagen fiber microstructure changes during pressurization in aortic media. Biomech. Model. Mechanobiol. 16 (3), 763–773.

Thorpe, C.T., Birch, H.L., Clegg, P.D., Screen, H.R., 2013. The role of the non-collagenous matrix in tendon function. Int. J. Exp. Pathol. 94 (4), 248–259.

Van Zandvoort, M., Engels, W., Douma, K., Beckers, L., Oude Egbrink, M., Daemen, M., Slaaf, D.W., 2004. Two-photon microscopy for imaging of the (atherosclerotic) vascular wall: a proof of concept study. J. Vasc. Res. 41 (1), 54–63.

Wan, W., Dixon, J.B., Gleason, R.L., 2012. Constitutive modeling of mouse carotid arteries using experimentally measured microstructural parameters. Biophys. J. 102 (12), 2916–2925.

Wang, R., Brewster, L.P., Gleason, R.L., 2013. In-situ characterization of the uncrimping process of arterial collagen fibers using two-photon confocal microscopy and digital image correlation. J. Biomech. 46 (15), 2726–2729.

Wenger, M.P., Bozec, L., Horton, M.A., Mesquida, P., 2007. Mechanical properties of collagen fibrils. Biophys. J. 93 (4), 1255–1263.

Zeinali-Davarani, S., Wang, Y., Chow, M.J., Turcotte, R., Zhang, Y., 2015. Contribution of collagen fiber undulation to regional biomechanical properties along porcine thoracic aorta. J. Biomech. Eng. 137 (5), 051,001.

Zhang, L., Lake, S., Barocas, V., Shephard, M., Picu, R., 2013. Cross-linked fiber network embedded in an elastic matrix. Soft Matter 9 (28), 6398–6405.

Zisserman, A., 2014. Image Analysis Course – 2D Fourier Transforms And Applications.

Zulliger, M.A., Fridez, P., Hayashi, K., Stergiopulos, N., 2004. A strain energy function for arteries accounting for wall composition and structure. J. Biomech. 37 (7), 989–1000.